Coasting in live-bearing fish

Quicazan Rubio, Elsa; van Leeuwen, J. L. (Johan); van Manen, Klaas; Fleuren, Mike; Pollux, Bart J. A.; Stamhuis, Eize

Published in:
Journal of the Royal Society Interface

DOI:
10.1098/rsif.2018.0714

Publication date:
2019

INTERFACE

royalsocietypublishing.org/journal/rsif

Research

Cite this article: Quicazan-Rubio EM, van Leeuwen JL, van Manen K, Fleuren M, Pollux BJA, Stamhuis EJ. 2019 Coasting in live-bearing fish: the drag penalty of being pregnant. *J. R. Soc. Interface* **16**: 20180714.
http://dx.doi.org/10.1098/rsif.2018.0714

Received: 24 September 2018
Accepted: 14 January 2019

Subject Category:
Life Sciences–Earth Science interface

Subject Areas:
biomechanics

Keywords:
swimming, biomechanics, reproductive allocation, particle image velocimetry

Authors for correspondence:
Bart J. A. Pollux
e-mail: bart.pollux@wur.nl
Eize J. Stamhuis
e-mail: e.j.stamhuis@rug.nl

Electronic supplementary material is available online at https://dx.doi.org/10.6084/m9.figshare.c.4373015.

THE ROYAL SOCIETY PUBLISHING

Coasting in live-bearing fish: the drag penalty of being pregnant

Elsa M. Quicazan-Rubio[1], Johan L. van Leeuwen[1], Klaas van Manen[2], Mike Fleuren[1], Bart J. A. Pollux[1] and Eize J. Stamhuis[2]

[1]Experimental Zoology Chair Group, Department of Animal Sciences, Wageningen University & Research, De Elst 1, 6708 WD Wageningen, The Netherlands
[2]Faculty of Science & Engineering, University of Groningen, Nijenborgh 7, AG Groningen 9747, The Netherlands

EMQ-R, 0000-0002-7320-8924; JLvL, 0000-0002-4433-880X; MF, 0000-0002-3186-3840; BJAP, 0000-0001-7242-2630; EJS, 0000-0001-7746-2535

Swimming performance of pregnant live-bearing fish is presumably constrained by the additional drag associated with the reproductive burden. Yet, it is still unclear how and to what extent the reproductive investment affects body drag of the females. We examined the effect of different levels of reproductive investment on body drag. The biggest measured increase in body volume due to pregnancy was about 43%, linked to a wetted area increase of about 16% and 69% for the frontal area. We printed three-dimensional models of live-bearing fish in a straight body posture representing different reproductive allocation (RA) levels. We measured the drag and visualized the flow around these models in a flow tunnel at different speeds. Drag grew in a power fashion with speed and exponentially with the increase of RA, thus drag penalty for becoming thicker was relatively low for low speeds compared to high ones. We show that the drag increase with increasing RA was most probably due to bigger regions of flow separation behind the enlarged belly. We suggest that the rising drag penalty with an increasing RA, possibly together with pregnancy-related negative effects on muscle- and abdominal bending performance, will reduce the maximum swimming speed.

1. Introduction

Oviparous (egg-laying) and viviparous (live-bearing) females exhibit considerable body shape changes during egg-carrying and pregnancy, respectively, due to the increase in reproductive allocation (RA, the proportion of body mass dedicated to reproduction). Both egg-carrying and pregnancy have been shown to negatively affect the locomotor performance of females in a number of different taxa (e.g. invertebrates [1,2], reptiles [3–8], fish [9,10], birds [11,12] and humans [13]).

The causes for the lower locomotor performance can be divided into two non-mutually exclusive categories: physiological and physical. First, the extra energy required to provision eggs before fertilization (in oviparous animals) or nourish developing embryos during gestation (in viviparous animals) might lead to lower energetic investments towards the locomotor muscles, negatively affecting their contractile properties and power output [14]. Secondly, the additional reproductive mass may negatively affect a female's ability to accelerate, while an increase in body volume could increase body drag and limit axial bending, negatively influencing a female's general swimming performance [10,14].

The mode of locomotion (e.g. flying, running, crawling, swimming, etc.) and the medium through which animals move (e.g. air, water, sand) determines how reproduction affects female locomotion. In swimming animals, both egg-carrying and pregnancy have been shown to lead to lower fast-start escape and sustained swimming performances, which has been attributed (at least partly) to an increase in drag on the body caused by an increase in frontal (projection of the fish area on the transversal plane, FA) and wetted area (WA, area exposed to the fluid) [9,10,15–17].

Despite the presumed relevance of drag on the swimming performance of gravid and pregnant females, the effect of the reproductive investment on drag production and the understanding of how extra drag originates remains poorly understood. So far, the effect of pregnancy on drag production has been examined only for the bottlenose dolphin, *Tursiops truncatus* [18], where drag was derived from videos of freely coasting pre- and post-parturition females. Pregnancy altered the morphology and kinematics of the females, and increased their drag during coasting, diminishing their locomotor performance. However, these observations were limited to only two dolphins and the effect of their reproductive investment was not taken into account in the analyses. These two constraints, the low sample size and the difficulty of correlating female body shape change with litter size, can be circumvented by working with poeciliid live-bearing fish. As a result of their small body size and short life cycle, this family is a convenient model for the study of the effect of reproduction on swimming performance.

Poeciliid fish use a wide range of swimming motions [19], including the burst-and-coast swimming style, alternating undulations of the body and caudal fin (BCF) with unpowered coasting movements. During BCF swimming, some parts of the body surface contribute to drag, whereas others contribute to propulsion and these contributions vary over the swimming cycle. In this case, drag can potentially be computed (using computational fluid mechanics) as the sum of all the forces on the body surface that counteract forward motion, while those forces on the body surface that add to the forward motion add up to the net propulsion. General application of this approach in adult fish is, however, prohibited by the considerable computational efforts and the unavoidable inaccuracies imposed by the turbulent nature of the flow. On the other hand, in a coasting fish (with a constant body shape), drag is the net fluid force on the body which decelerates the fish, which in turn reduces the drag because drag depends approximately quadratically on coasting speed [20]. A coasting fish can be simulated reasonably well by a rigid body in a flow tunnel [21,22], and this set-up facilitates the direct measurement of drag. And although measurements on rigid bodies at constant speeds is a simplification of the decelerating coasting in real fish, this represents a first estimate of the drag produced by pregnant swimming fish.

We aim to fill the knowledge gap on the effects of RA on the drag production of aquatic gravid and pregnant fish, using *Poeciliopsis gracilis* (Heckel, 1848). This species is a member of the Poeciliidae, a family of live-bearing fishes with considerable increases in RA during gestation, ranging from 4.1% to over 35% of their body weight (brood sizes ranges from 1 to over 200 newborns [23]). We obtained morphological information of females throughout their pregnancy to construct a series of representative three-dimensional body models of females with different RA. We then measured the drag of each fish model in a flow tunnel at a series of speeds and visualized the flow around the body to identify if and how the expected differences in drag were reflected in differences in the associated flow patterns. Thus, we tested how the increase in RA affects drag and the flow separation along the body.

2. Material and methods

2.1. Biological aspects

For a detailed description about the fish rearing and husbandry see electronic supplementary material, S1 text. *Poeciliopsis gracilis* has a high RA at the start of its pregnancy because almost all the nutrients for the embryo are stored in the egg yolk prior to fertilization [24]. The females usually carry simultaneously about 2 l that differ in the stage of embryonic development, a reproductive strategy referred to as superfetation [23,25,26]. At delivery, a second litter is at about half-way its internal developmental time and a third one is about to start.

We used a total of 20 females to measure brood sizes over a period of 6–12 months. A subset of those females ($N_{\text{fish}} = 10$) were used to quantify RA and changes in three-dimensional body shape during one interbrood interval (IB, the period between two parturition events). Females were not fed for 16 h prior to measurements to minimize possible confounding effects on body shape from food in the gastrointestinal tract. We focused on three stages of the interbrood interval: (i) the start of the interbrood interval (mean $\pm$ s.e.: 0.8 ± 0.1 days after delivery of a brood; $N_{\text{fish}} = 10$), hereafter referred to as IB = 0, (ii) the midpoint of the interbrood interval (IB = 0.5) and (iii) the end of the interbrood interval (mean $\pm$ s.e.: 1.6 ± 0.3 days before the delivery of the next brood; IB = 1). We measured the body volume before and shortly after the female delivered the offspring and expressed the differences between these volumes as a percentage of the female volume after delivery. We called this percentage the *reproductive allocation increase* (RAI).

A positive linear relationship between RAI and the number of newborns of these 10 females during one IB (figure 1*a*, grey bars) appeared to be significant (figure 1*b*, $p < 0.05$, $R^2 = 0.516$), indicating that the most developed litter has a dominant influence on the volume growth of the female. This correlation also allows a (rough) estimate of the effect of number of embryos in the oldest litter on body drag (see below). We also documented the clutch sizes of all the experimental population ($N_{\text{fish}} = 20$) for at least 6 months up to maximally 1 year and they produced clutch sizes varying between 1 and 48 newborns (figure 1*a*, black bars), a range positioned within the natural one (1–70 newborns, [27], BJA Pollux & DN Reznick 2010, unpublished data).

2.2. Three-dimensional model construction

We quantified body shape ($N_{\text{fish}} = 10$) by taking photographs from three perpendicular views (lateral, ventral and frontal; electronic supplementary material, figure S2*a*), following the method used by Fleuren *et al*. [17] and Voesenek *et al*. [28]. The outlines obtained (figure 2*a*; electronic supplementary material, figure S2*b*), were subsequently fitted with a series of 100 evenly spaced cross-sectional area ellipses along the body, whose major and minor axes were assigned as local height and width of the outline respectively. We excluded the fins to avoid confounding effects to our data due to their variable shape during swimming (e.g. due to folding and unfolding or bending of the fins).

Body posture appeared to be different during coasting than when at rest, namely in opercular abduction and orientation of the caudal peduncle (electronic supplementary material, figure S2*c*,*d*,*e*). Detailed series of pictures from the body could only be made when a fish was at rest. Thus, we corrected for the opercular abduction and caudal peduncle downward bending to get the closer representation of the body shape during coasting (see electronic supplementary material, S2 text for detailed information regarding body posture corrections).

The model representing IB = 0 was built by averaging width and height of the 100 sections ($N_{\text{fish}} = 10$). We then calculated the average of the differences in width and height along the body between segments IB = 0 and IB = 0.5, and between IB = 0 and IB = 1 (figure 2*b*). During pregnancy, the changes in height and width of the ellipses representing the head and peduncle were below 0.023% of the standard length (SL) of the fish. Because these two regions are not expected to change in size during pregnancy, we set this value as the threshold and any changes below it were considered non-significant and set to zero. We smoothed the

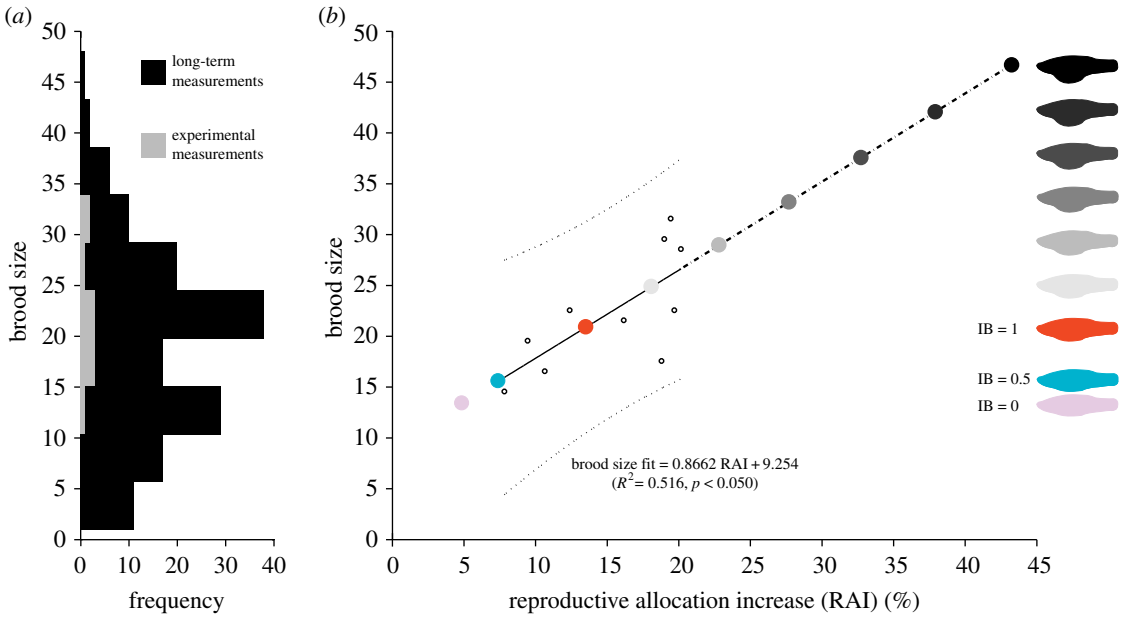

Figure 1. Brood size and RAI relationship. (*a*) Brood size frequency. Black squares: frequencies for $N_{fish} = 20$ examined through multiple interbrood intervals. Grey squares: frequencies for $N_{fish} = 10$ in the experimental interbrood interval. (*b*) Linear regression of brood size and RAI from beginning to the end of one interbrood interval of $N_{fish} = 10$ (small open circles). Dotted lines represent 95% confidence intervals. Fish profiles represent the full range of the population's brood sizes, built by extrapolating the linear regression. The bottom 3 models [light purple, blue and orange] represent IB = 0, 0.5 and 1, respectively. The remaining fish models represent bigger broods modelled by adding 1.5, 2.0, 2.5, 3.0, 3.5 and 4.0 times the averaged change in width and height seen between IB = 0 and IB = 1 (see paragraph 2.2). (Online version in colour.)

resulting curves using a simple moving average filter with a window of five data points (using the MATLAB function 'moving' by Aslak Grinsted; electronic supplementary material, figure S3). We added the corresponding filtered data to the IB = 0 model to build the IB = 0.5 and IB = 1 (figure 2*c*). The external shape of the eyes could not be captured with the longitudinal series of ellipses that were used to quantify body shape. For each fish, the outer shape of both eyes was digitized from the images at IB = 0 and was modelled with a short series of super ellipses (for details see electronic supplementary material, S3). The averaged eye model for all females was merged with the head of each of the new models (one example in figure 2*d*).

The three average body models (IB = 0, IB = 0.5 and IB = 1) were derived from the subsample of our laboratory population ($N_{fish} = 10$). The brood sizes and RAs in that subsample were rather small (ranging from 14 to 31), smaller than those observed for the full population over several interbrood intervals (ranging up to 48 babies). To account for this variation, we linearly extrapolated the relationship between brood size and body RAI (brood size fit = 0.8662 RAI + 9.254) and built an additional six body models representing the range of brood sizes and body volumes of the laboratory population (figures 1*b* and 2*e*). These models were obtained by adding to the IB = 0 model the difference in width and height between IB = 0 and IB = 1, multiplied by 1.5, 2, 2.5, 3, 3.5 and 4 (figure 2*e*). Because the dorsal outline shows only minor changes throughout pregnancy, we kept its shape constant among models (figure 2*e*). We used the same eye model for all fish models.

We constructed a total of nine fish models (RAI = 4.8, 7.4, 13.5, 18.1, 22.8, 27.7, 32.7, 37.9 and 43.2) by means of three-dimensional printing. The trunk was shaped by generating ellipses with the heights and widths for each model. The ellipses along the body were implemented in stereolithography (STL) meshes. We resized the models to optimize them for the flow and force measurements, given the tunnel dimensions and specifications of the force transducer. All meshes were scaled at 1:3.2 using the averaged SL of the fish (mean ± s.d.: 0.0474 ± 0.0029 m), resulting in models of 15 cm length. A hole was modelled on the dorsal side on top of the centre of mass of the fish model to fit a carbon-fibre rod (diam. 5 mm). Physical models were three-dimensional printed with Polyamide PA 2200 on a selective laser sintering printer (EOS Formiga P 100), with 0.1 mm resolution.

To measure the effect that surface texture and the shape from a single pregnant fish would have on the drag production, we photographed an additional (11th) female in the same way as described above, and 1–2 days before anticipated delivery we sacrificed it using an overdose of anaesthetic (Tricaine-S, MS-222) and weighed it. We then mounted the female by hanging it straight from the tail, froze it in liquid nitrogen and scanned it with a micro-CT scanner (Phoenix v[tome] × m of General Electric; voxel size 28.8 μm^3). From the CT images, a mesh of the fish was reconstructed using AVIZO® Fire software. Cleaning and further processing of the mesh was performed in Blender 2.72b. We digitally removed the fins, restored the eyes and took the lateral half that was least affected by the mounting and scanning processes and duplicated it to build a symmetrical model that represented the body shape during coasting. The mesh was treated similar to those of the other models to obtain a printed three-dimensional model.

To describe the body shape of the resulting 11 models, we computed the WA and maximum FA (electronic supplementary material, figures S4*a* and 5*b*) from the mesh information in Blender 2.72b. To refer to the body's streamlining, we used the fineness ratio (FR = standard length/max. height, von Mises 1945, electronic supplementary material, figure S4*b*). The fineness ratios of our fish models (FR = 2.97–3.80) overlapped well with the range found in natural *P. gracilis* populations (FR = 2.92–4.28, derived from data in [27]). SL and maximum height were obtained from the mesh information in Blender. None of these variables were used in the statistical analyses due to their correlation with volume increase. They were used to explain possible causes of the differences in drag (F_D), drag coefficient (C_D, i.e. drag normalized to reference area and the square of flow speed with respect to the object times 0.5 [22]), and flow behaviour.

2.3. Force measurements

We used the 300 l flow tunnel described in [22] (see electronic supplementary material, S4 text for details). Models were submerged in the middle of the cross section of the tank and attached (by a rod)

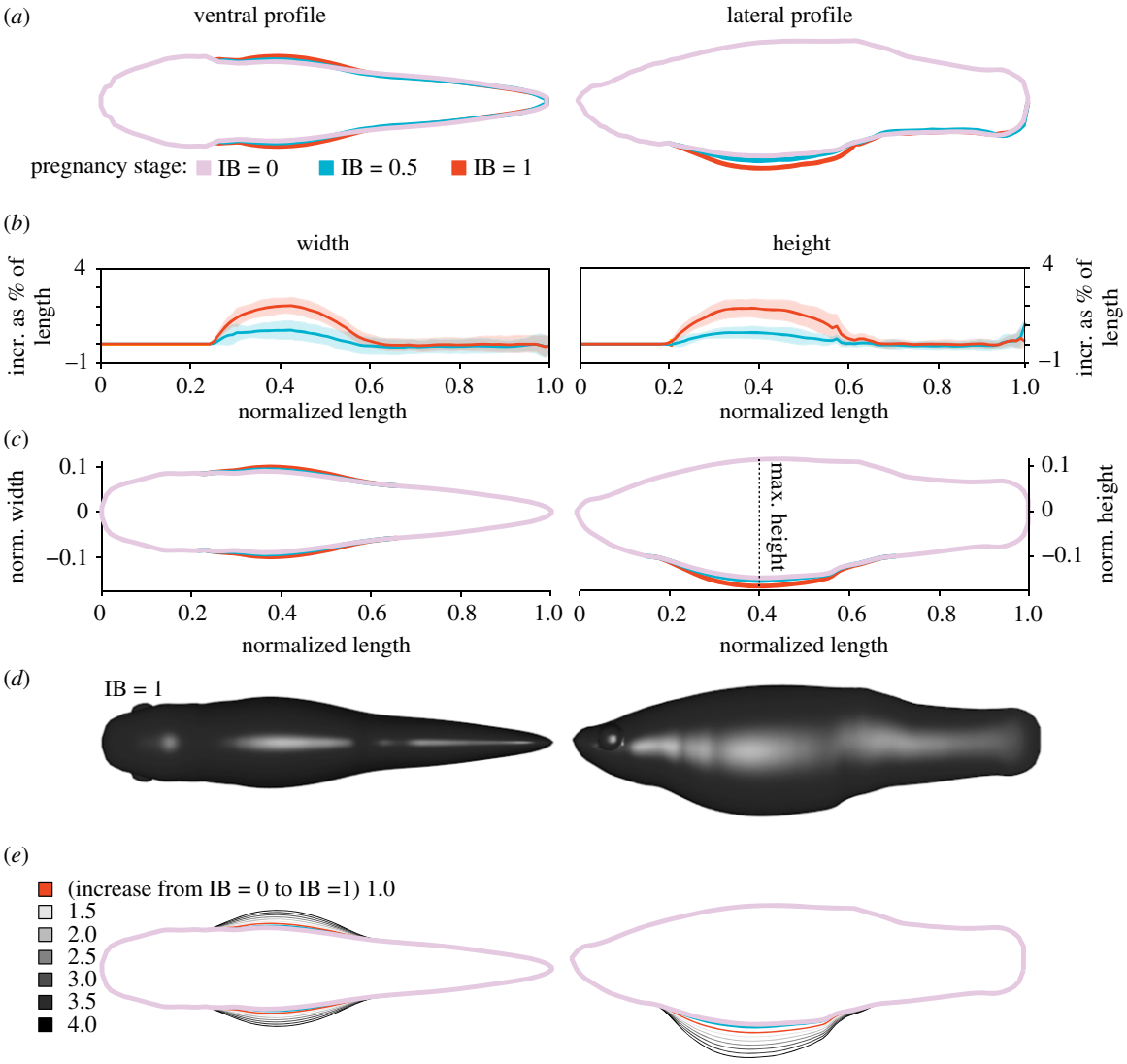

Figure 2. Construction of models based on body shapes of $N_{fish} = 10$ followed through one interbrood interval: IB = 0 (1–2 days after delivery, innermost [light purple] curve). IB = 0.5 (mid-time of the interval, middle [blue] curve). IB = 1 (1–2 days before delivery, external dark [orange] curve). (*a*) Width (left) and height (right) increase of one individual. (*b*) Along the body, mean and standard error of width and height increases with width and height ($N_{fish} = 10$). (*c*) Models IB = 0, IB = 0.5 and IB = 1. The latter two models were built by adding the mean width and height increases to the IB = 0 model. (*d*) Example of tested three-dimensional model, representing IB = 1. (*e*) Lateral and ventral view of extrapolated models built after adding changes in width and height to the IB = 0 model (specified in main text). (Online version in colour.)

to a force-measuring platform above the tank. On top of the platform, a force sensor (Honigmann GmbH RFS® 150-XY, Nr.705052, *x* : 5 N, *y* : 5 N, 1 mV V^{-1}) was mounted which was connected to a computer using an electronic precision measuring amplifier Tensiotron® TS 621. Data were recorded with a sample frequency of 1000 Hz during 5 s per test using HCC-Easy data transfer, an analysis program for Honigmann tension sensors.

The 10 *P. gracilis* females in our study reached maximum speeds of approximately 35 SL s^{-1} in fast-start escape responses (EM Quicazan-Rubio *et al*. 2014, unpublished data). Because we cannot exclude that the species could reach higher speeds in nature, we included also some higher speeds (up to 50 SL s^{-1}; electronic supplementary material, table S1). To ensure the same flow patterns for the coasting live fish and the three-dimensional printed models, we kept the body shape and Reynolds number (*Re*) the same: i.e. we increased the size of the fish models, while decreasing the flow velocity in the tunnel to keep *Re* constant ([29], see electronic supplementary material, S4 text for details). *Re* represents inertial versus viscous effects in the flow and is described by the equation:

$$Re = \frac{UL}{v}, \tag{2.1}$$

where *U* is the 'free flow' speed, *L* is the characteristic length of the object and *v* is the kinematic viscosity of the water. For *L*, we used the SL of the fish (unit: m). The relatively large size of the fish model with respective to the actual fish allowed us to improve the accuracy of our drag and flow measurements. The experimental drag forces were expected to comply with the Rayleigh drag equation [20,22,30]:

$$F_D = \frac{1}{2}\rho A U^2 C_D, \tag{2.2}$$

where ρ is the density of water (1000 kg m^{-3}), *A* is in this case the WA and C_D is the drag coefficient dependent on shape. F_D measurements were converted to C_D using equation (2.2).

$$C_D \frac{2F_D}{\rho . U^2 . A}. \tag{2.3}$$

2.4. Statistical analysis

The effects of the pregnancy stages and increased reproductive investment on the drag forces and coefficients of drag were analysed with general linear models (GLM), using the proc MIXED procedure (SAS version 9.2; SAS Institute Inc., Cary, North Carolina, USA. 2007). Changes in drag over the different speeds were

Table 1. Type 3 test of fixed effects of F_D and C_D for RAI (RAI, reproductive allocation increase; *Re*, Reynolds number; Num DF, numerator degrees of freedom; Den DF, denominator degrees of freedom).

dependent variable	effect	Num DF	Den DF	*F*-value	Pr > *F*
F_D	RAI	8	540	4736.67	<0.0001
	speed	14	540	33470.2	<0.0001
C_D	RAI	8	540	218.89	<0.0001
	Re	14	540	2.71E11	<0.0001

assessed with repeated measures analyses of variance (RM-ANOVA) using fish model (nine levels, corresponding to all models except the CT-scanned: IB = 0, IB = 0.5 and IB = 1, as well as six levels of higher RAI) and water speed (15 levels; electronic supplementary material, table S1) as fixed effects, and the repetitions per measurement (5) as the subject effect [31]. Changes in C_D over the examined *Re* range were also assessed using RM-ANOVA, with fish model (nine levels: the same ones as for the F_D), and *Re* (15 levels; electronic supplementary material, table S1) included as fixed effects, and measurement repetitions (5) as the subject effect.

To measure the effect that surface texture and the shape from a single pregnant fish would have on the drag production, we examined the similarity of results between the CT-scanned model and the IB = 1 model because they have similar RA. We applied GLM as above. Changes in drag (F_D) over the different speeds were assessed with RMANOVA including fish model (two levels: IB = 1 and CT-scan), and water speed (15 levels; electronic supplementary material, table S1) and the interaction between both as fixed effects, and the repetitions per measurement (5) as the subject effect [31]. Changes in drag coefficient (C_D) over the different Reynolds numbers were also assessed using RMANOVA, with fish model (two levels: the same as for F_D), and *Re* (15 levels; electronic supplementary material, table S1) included as fixed effects, and the times each measurement was taken (5) as the subject effect.

For all analyses, we selected a Toeplitz covariance structure based on Akaike's information criteria (AIC). All the multiple comparisons were done using a Bonferroni adjusted comparison-wise error rate of p ($0.05/n$, with n being the number of comparisons). The analyses were performed on the raw data.

2.5. Particle image velocimetry

To visualize the flow behaviour around the abdomen, we performed particle image velocimetry (PIV; [32]) recordings at three (tunnel) speeds: 0.32 m s^{-1}, 0.56 m s^{-1} and 0.64 m s^{-1} over a selection of models that covered the sizes of the laboratory fish, RAI of 4.8, 13.5, 18.1, 27.7 and 43.2% and the CT-scanned model. We analysed the images with PIVlab [33], averaged the vector fields of 50 frames, and visualized the local velocities and the streamlines (see electronic supplementary material, S5 text for details).

3. Results

3.1. Body shape changes due to reproductive allocation increase

The body volume of pregnant females increased due to the growing embryos by nearly 13% (the increase in volume is equivalent to RAI) for the interbrood interval photographed on 10 females, and when extrapolated for the biggest brood documented in the population of 20 females (48 newborns), it corresponded to about a 43.2% increase (figure 1*b*). The increase in RA corresponded with the increase in WA and FA (electronic supplementary material, figure S4*a*). Wetted area increased faster ($WA = 5 \times 10^{-5}\,RAI + 0.0113$, $p < 0.0001$) but proportionally less (approx. 16% for the biggest RAI) than the FA ($FA = 2 \times 10^{-5}\,RAI + 0.0009$, $p < 0.0001$, approx. 69% for the biggest RAI). The streamlining of the females decreased linearly with increased volume ($FR = -0.0215\,RAI + 3.8565$, $p < 0.0001$; electronic supplementary material, figure S4*b*).

3.2. Drag

Both RAI and flow speed significantly affected drag production (table 1). Drag was significantly different among all pairwise comparisons of model fish along the tested velocities (figure 3*a*, $p < 0.0014$), except for the models with lower RAI, 4.8 and 7.4% (IB = 0 and IB = 0.5) that showed similar drag ($p = 0.0922$; non-significant after Bonferroni correction). This was probably due to the small change in abdominal size in the first half of the interbrood interval (figure 2*b*). We observed that for the same force there was a significant reduction in speed when RAI increased (figure 3*b*,*c*), and at high speeds drag increased more rapidly which is represented by closer isolines with steeper slopes in figure 3*c*.

3.3. Drag coefficient

There was a significant effect of RAI and of *Re* on the drag coefficient (table 1). For almost all the data points, C_D lowered with *Re*, following the expected tendency, and the drop became deeper with higher RAI (figure 3*c*,*e*; electronic supplementary material, S6*b*,*d*). Comparing among models, the higher RAI became, the quicker the C_D increased. This was more easily observed at a constant *Re* (e.g. dotted straight line in figure 3*d*,*e*), where the space between lines was smaller at low RAI at high RAI (figure 3*d*), which corresponds in figure 3*e* to the bigger space between the contour lines at low RAI than at high RAI. Thus, in general, thicker body shapes presented bigger differences in C_D than with thinner models.

3.4. Drag expressed in terms of RAI and *U*

To explain the relationship between drag and both *U* and RAI, we performed a curve fit of F_D from all models (except the CT-scanned model), RAI and *U*, running the least square method (LSM) in Gnuplot 4.0. We found that drag grows exponentially with respect to RAI and in a power fashion with *U*:

$$F_D(\mathrm{RAI}, U) = 0.0606320\, e^{0.02301000.\,\mathrm{RAI}}\, U^{1.8012}. \quad (3.1)$$

To calculate the fitted C_D we transformed equation (2.3) following equation (2.2):

$$C_D(\mathrm{RAI}, U) = \frac{2 \times 0.0606320\, e^{0.02301000.\,\mathrm{RAI}}\, U^{1.80120}}{\rho\,(4.6558^{-5}\,\mathrm{RAI} + 0.011265)\, U^2}. \quad (3.2)$$

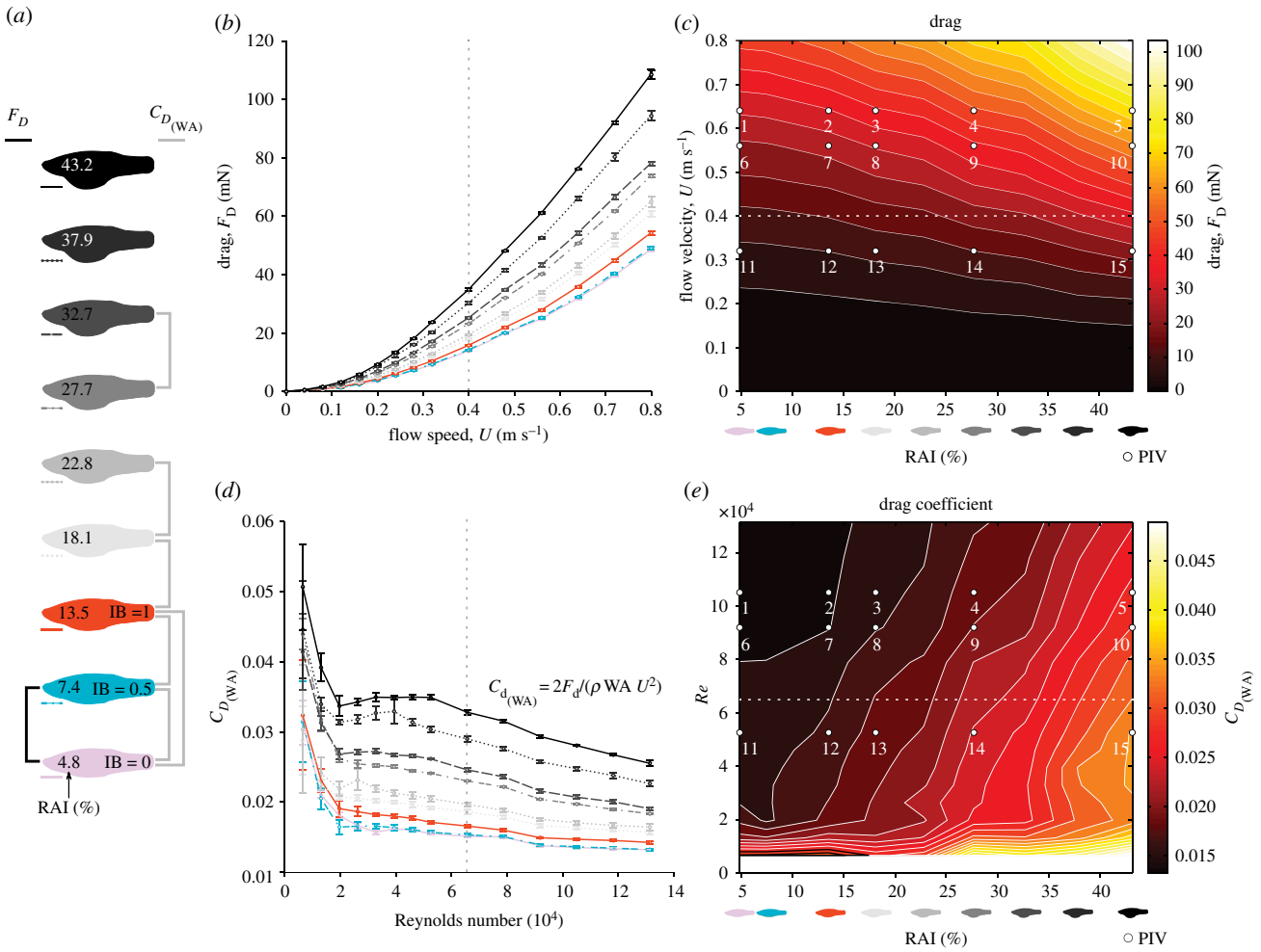

Figure 3. Raw data of F_D and C_D from models representing different RAI and tested at different U. (*a*) GLM analysis results of comparisons among models for F_D and C_D. The brackets represent the non-significant differences (Bonferroni adjusted comparison-wise error rate of $p(0.05/36) < 0.0014$). Brackets on the left show results for F_D, and on the right for C_D. (*b*) F_D results from the flow-tank experiments. (*c*) Contour plot of F_D as a function of U and RAI (obtained with cubic interpolation of the data set). (*d*) C_D calculated using equation (2.2) with WA. (*b,d*) Error bars represent the between-sampling standard error of the mean. Vertical dotted line represents equivalent speed and *Re*. (*e*) Contour plot of C_D as a function of *Re* and RAI. (*c,e*) White dots represent the RAI and the U at which PIV data were taken, corresponding to figure 4. Horizontal dotted line represents equivalent speed and *Re*. (Online version in colour.)

These equations allowed us to describe what happens beyond the limits tested, using just the experimental data (electronic supplementary material, figure S6).

3.5. Flow behaviour

All models showed separation of the boundary layer and the separation point was close to the anal region on the low RAI models and moved anteriorly when the RAI increased (figure 4). The size of the separation region increased with RAI, which corresponds to higher C_D, and for each model, this region became smaller at higher speeds, which corresponded to lower C_D, as expected [34]. We also observed that the region of separated flow presented the highest differences in local speeds within the region of interest (figures 4 and 5*d*).

3.6. Comparison between CT-scan model and averaged model with similar reproductive allocation

The CT-scan of an actual fish had a 5.6% larger FA, a 9.4% larger WA than the IB = 1 model (figure 5*bi*) possibly due to the replica of the scales and some differences in overall shape: e.g. it was less streamlined (FR of CT-scan model was 3.39, and of the IB = 1 model was 3.55, figure 5*bii*). There were no significant differences in drag for speeds up to approximately 0.6 m s^{-1}, which were the ones used by our population. Beyond that speed, the drag from the CT-scan model was significantly lower (at tunnel speed of 0.64 m s^{-1}, $p = 4.42 \times 10^{-5}$; 0.72 m s^{-1}, $p = 8.30 \times 10^{-10}$; and 0.80 m s^{-1}, $p = 1.08 \times 10^{-6}$, all significant after Bonferroni correction (figure 5*ci*)). The drag coefficients of both the CT-scan and IB = 1 model decreased with increased Reynolds number (figure 5*cii*) and were not significantly different over the examined speed range (electronic supplementary material, table S2 and figure 5*cii*). The flow visualization in figure 5*di–iii* suggested that a large portion of the drag was coming from the region behind the abdomen, where the higher differences in local speeds and therefore in pressures were expected. The flow follows the contour for most of the length of the fish, but the boundary layer separates around the anus on both models (figure 5*d*). The region of separated flow has a similar size among the speeds tested and between both models, but it has a laminar tendency on the CT-scan model whereas it presents whirls adjacent to model IB = 1.

4. Discussion

During pregnancy, aquatic animals are expected to experience greater drag forces due to an increased frontal area and surface-to-volume ratio [9,10,30]. Our study is the first to quantify the

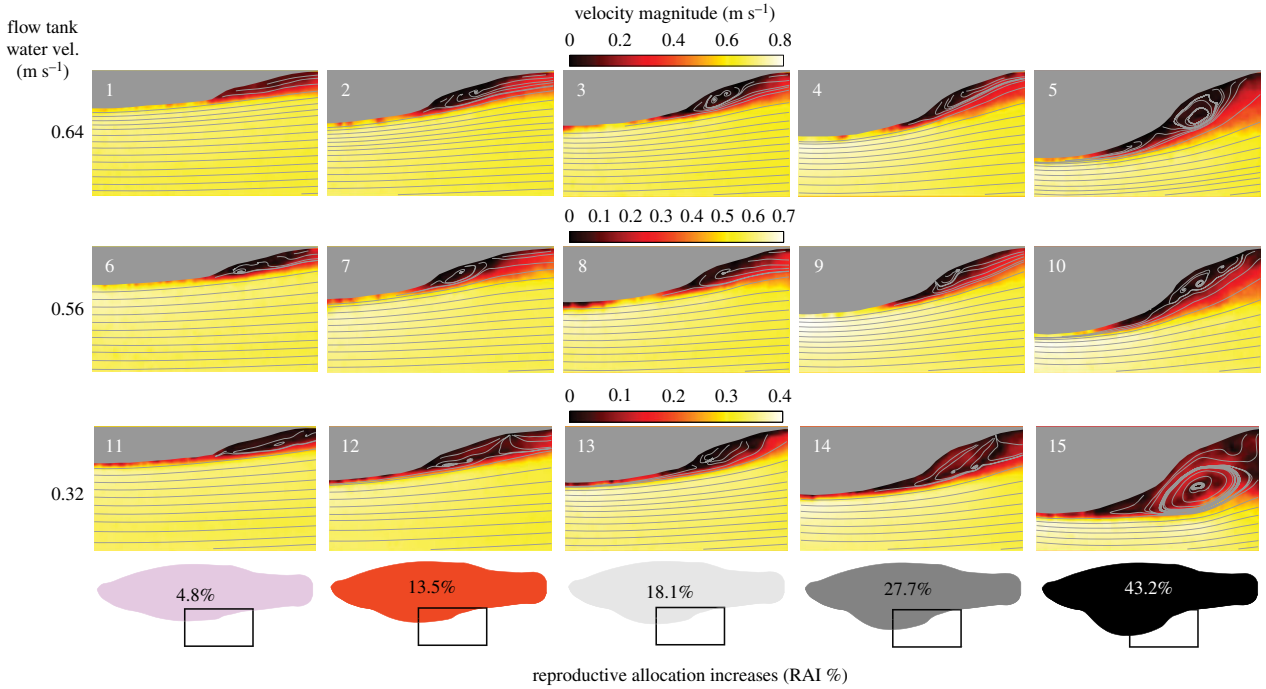

Figure 4. Flow fields recorded in flow tank from models representing different increases in reproductive allocation, tested at 0.32, 0.56, and at 0.64 m s^{-1}, *Re* ~ 50 000, 90 000 and 105 000, respectively. The white numbers correspond to the locations in figure 3*c*,*e*. (Online version in colour.)

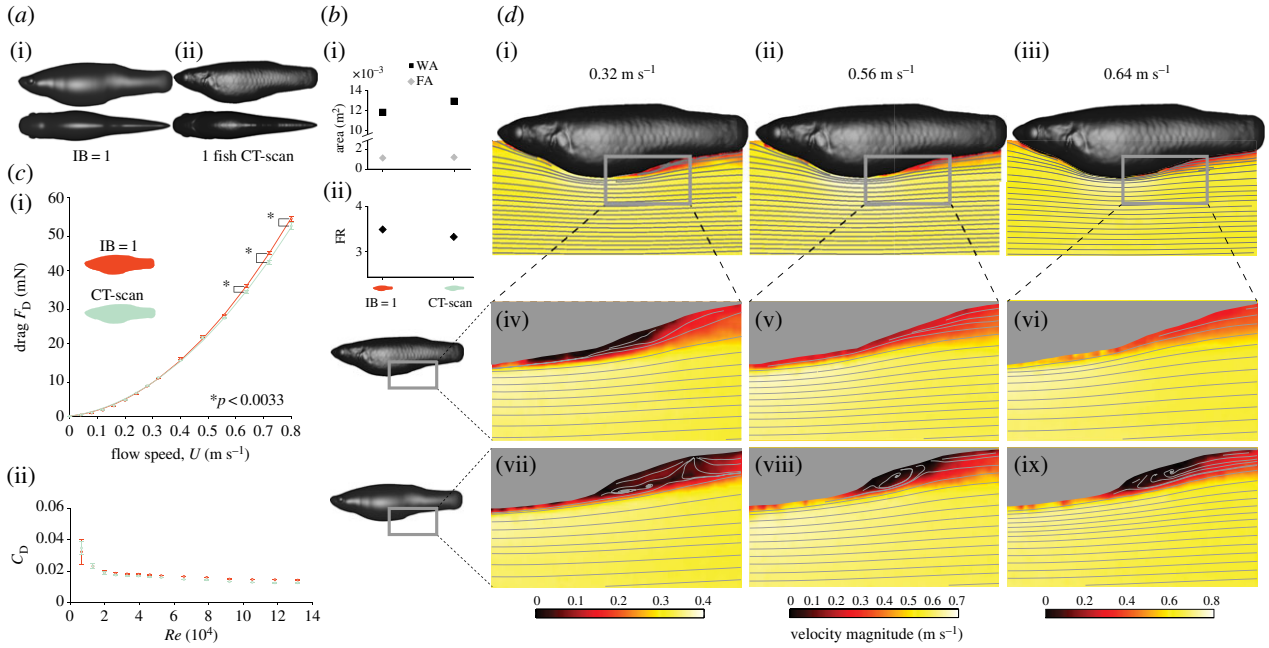

Figure 5. Comparison between models representing similar reproductive allocation. (*a*) Lateral and ventral view of models, (*ai*) model IB = 1, (*aii*) model from the CT-scan of 1 fish. (*b*) Models shape, (*bi*) cross-sectional (FA) and wetted area (WA), (*bii*) fineness ratio. (*c*) F_D, C_D and statistical results from the flow-tank experiments. Error bars represent the between-sampling standard error of the mean. (*ci*) F_D, * indicates significant differences using GLM analysis, comparing F_D within the same speed, between the two fish models. Bonferroni adjusted comparison-wise error rate of *P* (0.05/15) < 0.0033. Drag equation after polynomial regression for IB = 1: $F_{d\_fit} = 0.0744U^2 + 0.0085U$, $R^2 = 0.9997$, for Ct-scan: $F_{d\_fit} = 0.0682U^2 + 0.0103U$, $R^2 = 0.9993$ (*cii*) C_D. No significant differences were found between the two models. (*d*) Flow fields recorded in flow tank at 0.32, 0.56 and 0.64 m s^{-1}, equivalent to *Re* approximately 50000, 90000, 105 000, respectively. (*di*,ii,iii) CT-scan model from snout to tail. (*d*.iv,v,vi) Detail of abdomen and beginning of peduncle region of CT-scan model. (*d*vii,viii,ix) Detail of abdomen and beginning of peduncle region of model IB = 1. (Online version in colour.)

variations in drag due to changes in body shape in live-bearing fish. Specifically, we show that females 'pay a price' for (i) increasing their RA and/or (ii) swimming at higher speeds: drag grows exponentially with RA and in a power fashion with speed. We furthermore identified the increment in size of the region of flow separation as the cause of the extra drag when the RA grows bigger.

4.1. Body shape changed during pregnancy

The biggest brood observed in our lab population caused an increase of about 43.2% in volume (RAI), 69% in FA, 16% in WA, 28% in maximum height (girth) and a decrease in 22% in FR (electronic supplementary material, figure S4). This roughly corresponds with values found in other pregnant live-bearing fish and aquatic mammals. The two pregnant

bottlenose dolphins studied by Noren *et al*. [18] experienced comparable increases in FA (43% and 69%, respectively) and girth (16% and 26%), and *Gambusia affinis* experienced an increase in FA of about 52% [10]. The findings in this study might therefore also be relevant to other live-bearing and gravid animals (fish, reptiles, mammals). They might also be pertinent to aquatic animals with disturbances in their body shape due to tags or entangled fishing gear, both of which increase the drag production and animals exhibit a lower swimming speed, circumventing the extra energetic costs associated with the extra drag [35,36].

4.2. F_D and C_D changed with RAI and U

Females pay a price for increasing RA and for increasing speed. Drag changed exponentially with RAI and in a power fashion with U (equation (2.3), figure 3*a*,*d* and S6*a*,*c*). It was proportional to $U^{1.8}$, close to the expected value of U^2, reflecting the inertial flow regime in which *P. gracilis* swims ($Re > 10^{3.5}$). We observed that for the same drag there was a significant reduction in speed when RAI increased and that this effect was more acute at higher speeds and higher RAI (figure 3*a*,*d*). The same tendency was observed for the C_D, it increased more sharply with increasing RAI, as it is seen in figure 3*e*, where the contour lines are closer together at higher RAI. For bottlenose dolphins, drag increased faster with speed ($U^{2.13}$ pre-parturition and $U^{2.17}$ post-parturition [18]), than for *P. gracilis*, which might be related to higher *Re* at which they swim.

4.3. Origin of the extra drag

We suggest that the differences in F_D between models are mainly due to the increase of flow separation with increasing RAI. And the differences in F_D between speeds are mainly due to the characteristics of the flow within the region of separated flow. When RAI increased, F_D and C_D increased too and the region of flow separation became bigger (figures 3 and 4), which indicates a higher rate of momentum transfer to the water and consequently less kinetic energy available, so the animal would be slowed down [37]. On the other hand, at a constant RAI and increased speed, F_D increased and C_D decreased, which was reflected by a sharp decrease in the wake width of the separated flow from 0.32 to 0.56 m s^{-1} and a similar wake width between 0.56 and 0.64 m s^{-1} (figures 3*c*,*e* and 4). This difference in the wake width may be due to the transition from laminar to turbulent flow that happens at the *Re* analysed with PIV (*Re* ~50 000–105 000). At around $Re = 100\,000$, the flow close to the surface becomes turbulent, and so the fluid momentum increases allowing the flow to follow further the surface before separating. This also abruptly decreases the wake width [29].

4.4. Consequences of higher drag

Because pregnancy alters body shape, drag has been proposed to cause a considerable decrease in swimming performance of gravid and pregnant aquatic females such as bottlenose dolphins [18], short-horn sculpin [14] and aquatic snakes [5,38]. Poeciliid females at advanced stages of pregnancy also showed impaired locomotor performance [9,10] and we have demonstrated how drag augments considerably with RA, supporting the hypothesis that drag might be one of the main causes of poorer swimming performance of pregnant females, presumably together with lower muscle performance and limited axial bending, although the last two have not been proven yet.

4.5. Other aspects of pregnancy and fish swimming

In this study, we quantified drag forces on stiff, three-dimensional printed fish models placed in a flow tunnel. However, other biomechanical, physiological or behavioural aspects of fish swimming under natural conditions are likely to influence the production of drag.

First, *P. gracilis* has a burst and coast swimming style, making alternating undulations of its BCF, with unpowered coasting movements [39]. We studied the coasting phase of swimming by measuring the drag forces produced by rigid bodies and found significant differences with increasing RA. It has been computed that the drag forces for undulatory swimming are about three times higher than for rigid bodies [20], for two reasons: first, the undulating body causes a thinner boundary layer, increasing friction drag; second, the transverse recoil of the body caused by the lateral movement of the tail, produces extra drag when the tail resists the recoil movement [40]. Bending would be limited in pregnant fish by both the decrease of muscle/body ratio and the increase in FA in the abdominal region. It is difficult to predict the exact behaviour of the drag production for complete burst-and-coast cycles on live untethered fish that might also change in flexural stiffness throughout pregnancy [9]. Nevertheless, we expect that the scaling of drag, depending on RAI and speed that we found, may be indicative for the undulatory swimming as well.

Second, the presence of non-active fins in coasting live fish might cause small alterations to the production of drag. Furthermore, during coasting in the inertial regime, the changes in body shape have a marked effect on drag that overtakes the effect of fins posture [41]. In the case of the anal fin, which is located in the region where flow separation takes place, this may affect the flow pattern in this region. The fin is, however, abducted and oriented flat in the sagittal plane when in a neutral position and will therefore hardly interact with the separated flow. In such a posture it theoretically may dampen or redirect three-dimensional (out-of-plane) flow components in the separation region but this will be similar between models and have a small to probably negligible effect on the overall drag compared to the differences caused by changes in RAI, similar to what has been observed in zebrafish for differences in body shape [41].

Third, the characteristics of the skin surface such as compliance, and the presence of mucus and scales, might alter the production of drag on live fish [21]. Mucus could reduce drag by increasing the thickness of the boundary layer [42] and in some fish it can reduce C_D by up to 10% [43]. We observed that the model built after the CT-scanned images (figure 5) produced significantly lower drag at speeds above the ones used by our population of *P. gracilis* (figure 5*ci*). We could attribute this difference to the surface roughness and the body shape of the CT-scan model. Although we cannot discriminate the influence of each individual characteristic, it is possible that at relatively high speeds, the surface roughness facilitates keeping the boundary layer attached further against an adverse pressure gradient before separating [44]. However, at the speeds used by our population, it seems that neither the surface texture, nor the slight difference in body shape between the two models had a significant influence on the production

of drag, but more detailed tests on the interaction of surface texture and body shape effects on drag are needed. Nevertheless, models like the ones used in this study represent the production of drag based on RAI and U avoiding the technical difficulties of measuring on untethered live individuals at the right reproductive stages.

Fourth, muscles power locomotion, and their output limits the swimming performance of a wide variety of fish [45]. During pregnancy there is an excess allocation of energy to eggs and developing embryos, due to the mobilization of energy reserves and proteins from muscles and organs such as the liver to the gonads [46], and reflected on a significant increase in oxygen consumption [47,48] (except during BCF swimming in *P. reticulata*, where fin movement is a strong determinant of the oxygen consumed [19]). There might be also a decreased ratio of skeletal muscle mass to body mass, muscle disuse and physical stretch [14]. All of the above may negatively influence the contractile properties of the muscles and decrease power output throughout the cycle as have been found for gravid fish where the maximum isometric force and maximum power output decrease by 35% and 36%, respectively [14]. The power required to overcome drag and produce thrust at higher velocities increases sharply because power is proportional to U^3 [44,49]. While we did not study muscle performance, a restricted allocation of energy to the muscles may limit the power females can produce, further limiting the speed they can potentially attain at a given RAI during their pregnancy.

Finally, higher drag might decrease fast-start escape performance, possibly increasing a female's risk of predation [50], and it could also reduce the sustained swimming performance, limiting their ability to inhabit fast-flowing parts of the river [51]. Gravid and pregnant females may adjust their behaviour to avoid situations in which high locomotor performance is demanded. For example, some snakes and lizards have been shown to respond to a decrease in escape performance during gestation by relying more on crypsis to avoid predation (e.g. garter snake, *Thamnophis ordinoides* and common lizard *Zootoca vivipara*) [3,38], while pregnant guppies (*P. reticulata*) respond to a lower sustained swimming performance by displaying a micro-habitat shift, preferentially inhabiting shallow areas in the river that are characterized by low water flow velocities [51].

In conclusion, our results showed that the increase in females' volume due to the developing embryos, and/or the increase in swimming speeds, significantly increase the production of drag. This effect was consistent with a bigger region of flow separation located behind the abdomen. Drag grew in a power fashion with speed and exponentially with the increase of RA, thus drag penalty for becoming thicker was relatively low for low speeds compared to high ones. We suggest that this will cause the females' maximum swimming speed to decrease with RA. The effects of higher drag might be even worsened by a negative effect of pregnancy on muscles and abdominal bending performance.

Ethics. The experiments were approved by the Wageningen University Animal Experiments Committee. Permit number 2013103.

Data accessibility. Data are available from the Dryad Digital Repository: http://dx.doi.org/10.5061/dryad.4c039m4.

Authors' contributions. E.M.Q.-R, J.L.v.L., E.J.S., K.V.M. and B.J.A.P. conceptualized the experiment, E.M.Q.-R., E.J.S. K.V.M., J.L.v.L. and M.F. designed the experimental methodology (hardware and software). E.M.Q.-R. performed the experiments and analysed the data, E.M.Q.-R. wrote the first draft of the manuscript with input from J.L.v.L., B.J.A.P., M.F. and E.J.S. All authors provided feedback on the manuscript.

Competing interests. We declare we have no competing interests.

Funding. This study was supported by Doctorados en el Exterior de COLCIENCIAS, Convocatoria grant (no. 512 de 2010) to E.M.Q.-R., NWO-ALW Open Programme grant (821.02.024) to J.L.V.L. and VIDI grant (864.14.008) of the Netherlands Organisation for Scientific Research (NWO) to B.J.A.P.

Acknowledgements. We thank David Reznick for providing stocks of *Poeciliopsis gracilis*. We also thank T. Wiegers-Van der Wal, S. Visser, W. Nusselder, E. Roux, J. Lengkeek and M. ter Veld for their efforts regarding fish care, Dennis Worst for his help testing the experimental set-up, and Cees J. Voesenek for his help with the custom-made body model MATLAB routine. We appreciate the insightful feedback on the methodology from members of the Experimental Zoology Group at Wageningen University and of the Ocean Ecosystem group at the University of Groningen and from Luis García Rueda, Jan Wouter Kruyt and Daniel Quicazan. We also thank Mauricio Torres Mejía for his comments on a previous version of the manuscript.

References

1. Winfield IJ, Townsend CR. 1983 The cost of copepod reproduction: increased susceptibility to fish predation. *Oecologia* **60**, 406–411. (doi:10.1007/BF00376860)
2. Isaacs R, Byrne DN. 1998 Aerial distribution, flight behaviour and eggload: their inter-relationship during dispersal by the sweetpotato whitefly. *J. Anim. Ecol.* **67**, 741–750. (doi:10.1046/j.1365-2656.1998.00236.x)
3. Bauwens D, Thoen C. 1981 Escape tactics and vulnerability to predation associated with reproduction in the lizard *Lacerta vivipara*. *J. Anim. Ecol.* **50**, 733–743. (doi:10.2307/4133)
4. Garland TJ, Else PL. 1987 Seasonal, sexual, and individual variation in endurance and activity metabolism in lizards. *Am. J. Physiol.* **252**, R439–R449.
5. Seigel RA, Huggins MM, Ford NB. 1987 Reduction in locomotor ability as a cost of reproduction in gravid snakes. *Oecologia* **73**, 481–485. (doi:10.1007/BF00379404)
6. Shine R. 2003 Effects of pregnancy on locomotor performance: an experimental study on lizards. *Oecologia* **136**, 450–456. (doi:10.1007/s00442-003-1281-9)
7. van Damme R, Bauwens D, Verheyen RF. 1989 Effect of relative clutch mass on sprint speed in the lizard *Lacerta vivipara*. *J. Herpetol.* **23**, 459. (doi:10.2307/1564069)
8. Lourdais O, Brischoux F, DeNardo DF, Shine R. 2004 Protein catabolism in pregnant snakes (*Epicrates cenchria maurus* Boidae) compromises musculature and performance after reproduction. *J. Comp. Physiol. B* **174**, 383–391. (doi:10.1007/s00360-004-0424-6)
9. Ghalambor CK, Reznick DN, Walker JA. 2004 Constraints on adaptive evolution: the functional trade-off between reproduction and fast-start swimming performance in the Trinidadian guppy (*Poecilia reticulata*). *Am. Nat.* **164**, 38–50. (doi:10.1086/421412)
10. Plaut I. 2002 Does pregnancy affect swimming performance of female mosquitofish, *Gambusia affinis*? *Funct. Ecol.* **16**, 290–295. (doi:10.1046/j.1365-2435.2002.00638.x)
11. Veasey JS, Houston DC, Metcalfe NB. 2001 A hidden cost of reproduction: the trade-off between clutch size and escape take-off speed in female zebra finches. *J. Anim. Ecol.* **70**, 20–24. (doi:10.1111/j.1365-2656.2001.00476.x)
12. Lee SJ, Witter MS, Cuthill IC, Goldsmith AR. 1996 Reduction in escape performance as a cost of

reproduction in gravid starlings, *Sturnus vulgaris*. *Proc. R. Soc. Lond. B* **263**, 619–623. (doi:10.1098/rspb.1996.0093)

13. Wu W, Meijer OG, Lamoth CJC, Uegaki K, van Dieën JH, Wuisman PIJM, de Vries JIP, Beek PJ. 2004 Gait coordination in pregnancy: transverse pelvic and thoracic rotations and their relative phase. *Clin. Biomech.* **19**, 480–488. (doi:10.1016/j.clinbiomech.2004.02.003)
14. James RS, Johnston IA. 1998 Influence of spawning on swimming performance and muscle contractile properties in the short-horn sculpin. *J. Fish Biol.* **53**, 485–501. (doi:10.1006/jfbi.1998.0722)
15. Booth RK. 1998 Swimming performance of anadromous Atlantic salmon, *Salmo salar* L., during their spawning migration in the Exploits River, Newfoundland, Canada. PhD thesis, University of Waterloo, Waterloo, ON, Canada.
16. Belk MC, Tuckfield RC. 2010 Changing costs of reproduction: age-based differences in reproductive allocation and escape performance in a livebearing fish. *Oikos* **119**, 163–169. (doi:10.1111/j.1600-0706.2009.17742.x)
17. Fleuren M, Quicazán-Rubio EM, van Leeuwen JL, Pollux BJA. 2018 Why do placentas evolve? Evidence for a morphological advantage during pregnancy in live-bearing fish. *PLoS ONE* **13**, e0195976. (doi:10.1371/journal.pone.0195976)
18. Noren SR, Redfern JV, Edwards EF. 2011 Pregnancy is a drag: hydrodynamics, kinematics and performance in pre- and post-parturition bottlenose dolphins (*Tursiops truncatus*). *J. Exp. Biol.* **214**, 4151–4159. (doi:10.1242/jeb.059121)
19. Svendsen JC, Banet AI, Christensen RHB, Steffensen JF, Aarestrup K. 2013 Effects of intraspecific variation in reproductive traits, pectoral fin use and burst swimming on metabolic rates and swimming performance in the Trinidadian guppy (*Poecilia reticulata*). *J. Exp. Biol.* **216**, 3564–3574. (doi:10.1242/jeb.083089)
20. Alexander RM. 2003 *Principles of animal locomotion*. Princeton, NJ: Princeton University Press.
21. McHenry MJ, Lauder GV. 2005 The mechanical scaling of coasting in zebrafish (*Danio rerio*). *J. Exp. Biol.* **208**, 2289–2301. (doi:10.1242/jeb.01642)
22. van Wassenbergh S, van Manen K, Marcroft TA, Alfaro ME, Stamhuis EJ. 2014 Boxfish swimming paradox resolved: forces by the flow of water around the body promote manoeuvrability. *J. R. Soc. Interface* **12**, 20141146. (doi:10.1098/rsif.2014.1146)
23. Pires MN, Banet AI, Pollux BJA, Reznick DN. 2011 Variation and evolution of reproductive strategies. In *Ecology and evolution of poeciliid fishes* (eds JP Evans, A Pilastro, I Schlupp), pp. 28–37. Chicago, IL: The University of Chicago Press.
24. Reznick DN, Mateos M, Springer MS. 2002 Independent origins and rapid fish genus *Poeciliopsis*. *Science* **298**, 1018–1020. (doi:10.1126/science.1076018)
25. Turner CL. 1937 Reproductive cycles and superfetation in poeciliid fishes. *Biol. Bull.* **72**, 145–164. (doi:10.2307/1537249)
26. Scrimshaw NS. 1944 Superfetation in poeciliid fishes. *Copeia* **1944**, 180–183. (doi:10.2307/1437814)
27. Frías-Alvarez P, Zúñiga-Vega JJ. 2016 Superfetation in live-bearing fishes is not always the result of a morphological constraint. *Oecologia* **181**, 645–658. (doi:10.1007/s00442-015-3477-1)
28. Voesenek CJ, Pieters RPM, van Leeuwen JL. 2016 Automated reconstruction of three-dimensional fish motion, forces, and torques. *PLoS ONE* **11**, 8–10. (doi:10.1371/journal.pone.0146682)
29. Vogel S. 1994 *Life in moving fluids*, 2nd edn. Princeton, NJ: Princeton University Press.
30. Webb PW. 1975 Hydrodynamics and energetics of fish propulsion. *Bull. Fish. Res. Board Canada* **190**, 1–158.
31. Littell RC, Henry PR, Ammerman CB. 1998 Statistical analysis of repeated measures data using SAS procedures. *J. Anim. Sci.* **76**, 1216. (doi:10.2527/1998.7641216x)
32. Stamhuis EJ. 2006 Basics and principles of particle image velocimetry (PIV) for mapping biogenic and biologically relevant flows. *Aquat. Ecol.* **40**, 463–479. (doi:10.1007/s10452-005-6567-z)
33. Thielicke W, Stamhuis EJ. 2014 PIVlab - towards user-friendly, affordable and accurate digital particle image velocimetry in MATLAB. *J. Open Res. Softw.* **2**, e30. (doi:10.5334/jors.bl)
34. Anderson JD. 2001 *Fundamentals of aerodynamics*, 3rd edn. New York, NY: McGraw-Hill Companies.
35. van der Hoop JM. 2017 Effects of added drag on cetaceans: fishing gear entanglement and external tag attachment. PhD dissertation, Massachusetts Institute of Technology and Woods Hole Oceanographic Institution, USA.
36. Suzuki I, Sato K, Fahlman A, Naito Y, Miyazaki N, Trites AW. 2014 Drag, but not buoyancy, affects swim speed in captive Steller sea lions. *Biol. Open* **3**, 379–386. (doi:10.1242/bio.20146130)
37. Feldkamp SD. 1987 Swimming in the California sea lion: morphometrics, drag and energetics. *J. Exp. Biol.* **131**, 117–135.
38. Brodie III ED. 1989 Behavioral modification as a means of reducing the cost of reproduction. *Am. Nat.* **134**, 225. (doi:10.1086/284977)
39. Videler JJ, Weihs D. 1982 Energetic advantages of burst-and-coast swimming of fish at high speeds. *J. Exp. Biol.* **97**, 169–178.
40. Lighthill MJ. 1971 Large-amplitude elongated-body theory of fish locomotion. *Proc. R. Soc. Lond. B* **179**, 125–138. (doi:10.1098/rspb.1971.0085)
41. McHenry MJ, Lauder GV. 2006 Ontogeny of form and function: locomotor morphology and drag in zebrafish (*Danio rerio*). *J. Morphol.* **267**, 1099–1109. (doi:10.1002/jmor.10462)
42. Daniel TL. 1981 Fish Mucus: in situ measurements of polymer drag reduction. *Biol. Bull.* **160**, 376–382. (doi:10.2307/1540846)
43. Sagnes P, Champagne J-Y, Morel R. 2000 Shifts in drag and swimming potential during grayling ontogenesis: relations with habitat use. *J. Fish Biol.* **57**, 52–68. (doi:10.1006/jfbi.2000.1288)
44. Fish FE, Rohr J. 1999 Review of dolphin hydrodynamics and swimming performance. San Diego, CA: SPAWARS System Center Technical Report 1801. (doi:10. 21236/ADA369158)
45. Wakeling JM, Johnston IA. 1998 Muscle power output limits fast-start performance in fish. *J. Exp. Biol.* **201**, 1505–1526.
46. Love RM. 1980 *The chemical biology of fishes*. London, UK: Academic Press.
47. Karamushko LI, Christiansen JS. 2002 Aerobic scaling and resting metabolism in oviferous and post-spawning Barents Sea capelin *Mallotus villosus villosus* (Müller, 1776). *J. Exp. Mar. Bio. Ecol.* **269**, 1–8. (doi:10.1016/S0022-0981(01)00392-6)
48. Timmerman CM, Chapman LJ. 2003 The effect of gestational state on oxygen consumption and response to hypoxia in the sailfin molly, *Poecilia latipinna*. *Environ. Biol. Fishes* **68**, 293–299. (doi:10.1023/A:1027300701599)
49. Randall D, Burggren W, French K. 2002 *Eckert. Animal physiology. Mechanisms and adaptations*, 5th edn. New York, NY: W. H. Freeman and Company.
50. Walker JA, Ghalambor CK, Griset OL, McKenney D, Reznick DN. 2005 Do faster starts increase the probability of evading predators? *Funct. Ecol.* **19**, 808–815. (doi:10.1111/j.1365-2435.2005.01033.x)
51. Banet AI, Svendsen JC, Eng KJ, Reznick DN. 2016 Linking reproduction, locomotion, and habitat use in the Trinidadian guppy (*Poecilia reticulata*). *Oecologia* **181**, 87–96. (doi:10.1007/s00442-015-3542-9)